Advances in Nano Research, *Vol. 15, No. 2 (2023) 91-104*
https://doi.org/10.12989/anr.2023.15.2.091

Thin CNTs nanoliquid film development over a rough rotating disk

Swatilekha Nag[1a], Susanta Maity[*2] and Sanjeev K. Metya[3b]

[1]*Department of Mathematics, Pandit Deendayal Upadhyaya Adarsha Mahavidyalaya, Behali, Assam-784184, India*
[2]*Department of Basic and Applied Science, National Institute of Technology Arunachal Pradesh, Jote, Papum Pare-791113, India*
[3]*Department of Electronics and Communication Engineering, National Institute of Technology Arunachal Pradesh, Jote, Papum Pare-791113, India*

(*Received January 14, 2020, Revised February 22, 2023, Accepted May 30, 2023*)

Abstract. Development of thin carbon nanotubes (CNTs) nanoliquid film over the rough surface of a horizontal rotating disk is investigated by considering symmetric roughness either along the azimuthal or radial directions. The disk surface is either heated or cooled axisymmetrically from below. The effects of single-walled carbon nanotubes (SWCNTs), multi-walled carbon nanotubes (MWCNTs) are analyzed on the film thinning process with different types of base liquids. Closed form solutions for velocity and temperature field are obtained for small values of Reynolds number whereas the numerical solution is derived for moderate values of Reynolds number. It is found that fluid retention / depletion takes place when the roughness is symmetric along the azimuthal / radial directions. It is also seen that the film thinning rate enhances for MWCNTs compare to SWCNTs. Further it is found that two different heat transfer regions exits within the flow domain depending on the fact that heat is transferred from disk to liquid film and vice-versa.

Keywords: carbon nanotubes (CNTs); nanoliquid; rotating disk; thermocapillary flow; thin film

1. Introduction

In last two decades the study of nanofluid becomes major area of research among the scientists and technologists due to its enormous application in different technological processes. Nanofluid consists colloidal suspension of nanometer size metallic or non-metallic particles (diameters 1-100 nm) in the conventional heat transfer fluids like water, ethylene glycol, engine oil, etc. and these fluids have poor thermal performance. The suspension of tiny-sized particles in the conventional fluids shows much higher thermal conductivity of these fluids. For this reason, nanofluids have widespread industrial applications such as solar technology, cooling of electronic devices, cancer therapy, biomedicine, etc. Masuda *et al*. (1993) observed increase of thermal conductivity of a base fluid by dispersing ultra-fine particles of Al_2O_3, SiO_2 and TiO_2. The term nanofluid was first invented by Choi (1995) and showed the anomalous increase of thermal conductivity of the conventional fluids. Buongiorno (2006) modeled the laminar flow of nanofluids by taking effects of thermo-phoresis and Brownian motion in the convective heat transport problem. Niled and Kuznetsov (2009) examined the thermal instability of convective heat and mass transfer in an porous horizontal medium saturated by nanofluid. Later, Kumar *et al*. (2017) investigated unsteady MHD boundary layer flow of Casson fluid between two parallel disks with the effects of thermal radiation, thermophoresis and Brownian motion. Tlili *et al*. (2020, 2021) discussed the effects of nanoparticle shape on MHD ferrofluid film flow due to a stretching sheet in case of hybrid and mono nanofluids respectively. Carbon nanotube (CNT) is a graphene sheet rolled in to a cylinder with nanometer size diameter. The CNTs are classified in two groups namely single-walled carbon nanotubes (SWCNTs) and multi-walled carbon nanotubes (MWCNTs). A SWCNTs has only single graphene sheet while collection of nested tubes of continuously increasing diameters is termed as MWCNTs. Radushkevich and Lukyanovich (1952) and Iijima (1991) invented and described the structural properties of CNTs. Iijima and Ichihashi (1993) showed the properties of the new type of CNTs known as the single-walled carbon nanotubes. Later, numerous researchers Akbar *et al*. (2014), Wang *et al*. (2014), Akbar *et al*. (2015), Akbar and Butt (2015), Sidik *et al*. (2017) discussed the effects of heat transfer due to CNTs nanofluids.

The spin coating is a technique by which a very thin uniform layer of film (layers of paint, polymer, lacquer etc.) developed over the surface of a horizontal rotating substrate/ disk with the help of centrifugal force. In general, a small amount of liquid solution is deposited at the center of the disk with the help of a pipette or syringe. After that the disk starts to rotate, resulting liquid solution spreads uniformly on the entire surface of the disk by the action of centrifugal force. This technique is used in many industrial processes for manufacturing of integrated circuits, solar cells, insulators, nanomaterials, magnetic disk coatings, compact disks for data storage etc. The development of thin Newtonian liquid film over a spinning disk was first theoretically studied by Emslie *et al*. (1958). Washo (1977) examined the use of the spin coating technique in micro-electronics industry by his experimental as well as theoretical

*Corresponding author, Ph.D., Associate Professor
E-mail: susanta@nitap.ac.in
[a] M.Sc. Student
[b] Ph.D., Assistant Professor

ISSN: 2287-237X (Print), 2287-2388 (Online)

study. Myerhofer (1978) considered the effect of solvent evaporation in spin coating process. Mouhamad *et al*. (2014) investigated formation of polymer film through the spin coating process by assuming the viscosity as the function of concentration. Jenekhe and Schuldt (1984) studied the development of non-Newtonian power-law and Carreau liquid films on a rotating disk. Higgins (1986) first took the full set of Navier-Stoke Eqs. to investigate unsteady film flow on a rotating disk by the match asymptotic analysis. Dandapat and Roy (1990, 1994) considered the unsteady film flow over a hot / cold rotating disk with the thermocapillary effect. Later, Dandapat (2001) analyzed the crucial role of viscosity on film flow over a rotating disk. Wu (2001) investigated numerically the axisymmetrically thin film flow over a heated rotating disk with the lubrication approximation. Cregan and O'Brien (2013) derived the improved asymptotic solution for the spin-coating with a small evaporation. Karpitschka *et al*. (2015) discussed the vertical composition profile of evaporating polymer film in spin coating. Recently, Maity (2017) studied the nanoliquid film flow over a spinning disk with the thermocapillary effect. The thin double-layer viscous liquid film flow over a spinning disk with the different physical effects was investigated by McIntyre and Brush (2010), Sahoo *et al*. (2016), Dandapat and Singh (2015). Matsumoto *et al*. (1989) modelled the unsteady thin film development on a spinning disk with deformable free surface and studied the problem numerically. Later, Kitamura (2001), Dandapat *et al*. (2005), Usha *et al*. (2005), Dandapat and Maity (2009) studied the thin film development on a spinning disk under the assumption of deformable free surface with effects of surface tension variation, viscosity variation, flow instability, evaporation, external air flow, etc.

In all the above investigations it is assumed that the disk surface or topographical structure over the disk is wet so no-slip condition is applicable at every point on the solid surface. But during the coating of the substrates, one need to place the substrates over the disk either arranged in concentric rings or may be radially symmetric or mixed of these two. This placement of substrates over the disk leads to the roughness over the surface. Ma and Hwang (1990) analyzed the effects of surface roughness and air-shear on film development over a rotating disk. Through numerical solution they showed that: (i) the surface roughness increases significantly the retention of liquid on a rotating disk, (ii) the different topographic structure of the surface roughness asperities lead to the different asymptotic limits of the lubricant retention. But adequate attention has not been paid to this orderly roughness problem although many researchers Peurrung and Graves (1991), Usha and Gotz (2001) considered the flow of thin liquid film over a rough rotating disk. Miklavčič and Wang (2004) examined the Von Kármán (1921) problem of infinite viscous fluid over a rough rotating disk. Turkyilmazoglu (2010) considered the above problem for electrically conducting infinite fluid over a rough rotating disk. Recently, Dandapat *et al*. (2017) investigated the effects of surface roughness and air flow due to the thin film flow of two-fluids on a rotating disk.

In this paper, the flow of thin CNTs nanoliquid film over a spinning disk is investigated with the assumption that the disk surface is rough. The directions of roughness on the disk surface are either arranged radial symmetric or azimuthal, i.e., on a concentrically grooved disk such as a phonograph record or a laser-etched disk (See, Fig. 1). The initial film thickness is assumed to be uniform and it remains uniform throughout the spinning of the disk.

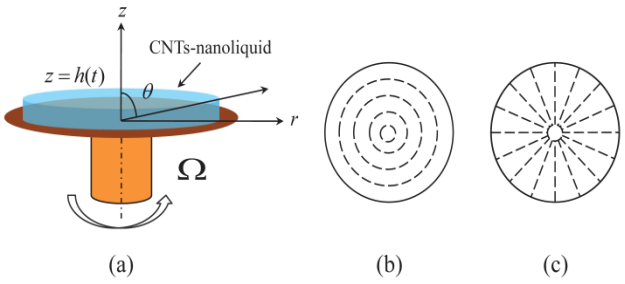

Fig. 1 Geometrical representation of the flow problem

2. Materials and methods

Unsteady, incompressible flow of CNTs nanoliquid film is considered over a rough horizontal rotating disk. The film thickness is assumed to be uniform h_0 and the radius is large compared with the film thickness. The CNTs nanoliquid consists of ethanol, methanol and ethylene-glycol as the base liquids and single-walled nanotubes (SWCNTs) and multi-walled carbon nanotubes (MWCNTs) as the nanoparticles. Choosing cylindrical-polar coordinate system (r,θ,z) with origin at center of the disk and z-axis is vertically upwards. Initially, disk is at rest and it starts to rotate with angular velocity Ω about the z-axis. Let (u,v,w) and $T$are respectively the velocity components and temperature of CNTs-nanoliquid. The axisymmetric Eq. of continuity, momentum and energy Eqs for nanoliquid flow over a rotating disk are as follows (see, Avramenko and Shevchuk (2022), Dandapat (2001), Maity (2017), Ellahi *et al*. (2018), Turkyilmazoglu (2014)):

$$\frac{\partial u}{\partial r}+\frac{u}{r}+\frac{\partial w}{\partial z}=0 \tag{1}$$

$$\rho_{nf}\left[\frac{\partial u}{\partial t}+u\frac{\partial u}{\partial r}+w\frac{\partial u}{\partial z}-\frac{v^2}{r}\right] = -\frac{\partial p}{\partial r}+\mu_{nf}\left[\frac{\partial^2 u}{\partial r^2}+\frac{\partial}{\partial r}\left(\frac{u}{r}\right)+\frac{\partial^2 u}{\partial z^2}\right] \tag{2}$$

$$\rho_{nf}\left[\frac{\partial v}{\partial t}+u\frac{\partial v}{\partial r}+w\frac{\partial v}{\partial z}+\frac{uv}{r}\right] = \mu_{nf}\left[\frac{\partial^2 v}{\partial r^2}+\frac{\partial}{\partial r}\left(\frac{v}{r}\right)+\frac{\partial^2 v}{\partial z^2}\right] \tag{3}$$

$$\rho_{nf}\left[\frac{\partial w}{\partial t}+u\frac{\partial w}{\partial r}+w\frac{\partial w}{\partial z}\right] = -\frac{\partial p}{\partial z}+\mu_{nf}\left[\frac{\partial^2 w}{\partial r^2}+\frac{1}{r}\frac{\partial w}{\partial r}+\frac{\partial^2 w}{\partial z^2}\right] \tag{4}$$

$$\left(\rho C_p\right)_{nf}\left[\frac{\partial T}{\partial t}+u\frac{\partial T}{\partial r}+w\frac{\partial T}{\partial z}\right] = k_{nf}\left[\frac{\partial^2 T}{\partial r^2}+\frac{1}{r}\frac{\partial T}{\partial r}+\frac{\partial^2 T}{\partial z^2}\right] \tag{5}$$

Table 1 Thermo-physical properties of different nano-particles and base liquid (see, Khan *et al*. (2020), Ellahi *et al*. (2018), Krishanan *et al*. (2020))

		ρ (kg/m^3)	C_p(J/kgK)	k(W/mK)	Pr
Base liquid	Methanol	790	2534	0.200	7.24
	Ethanol	789	2500	0.0235	1.53
	Ethylene-Glycol	1101	2400	0.256	204.0
Nano-particles	SWCNT	2600	425	6600	-
	MWCNT	1600	796	3000	-

where p is the pressure, ρ_{nf} is the density, μ_{nf} is the dynamic viscosity, $(\rho C_P)_{nf}$ is thermal conductivity and k_{nf} is the heat capacity of the nanoliquid. The above thermo-physical properties of the nanoliquid are defined as follows (see, Akbar *et al*. (2014), Khan *et al*. (2020), Haq *et al*. (2017)):

$$\rho_{nf} = (1-\phi)\rho_{bl} + \phi\rho_{CNT} \tag{6}$$

$$\mu_{nf} = \frac{\mu_{bl}}{(1-\phi)^{\frac{5}{2}}} \tag{7}$$

$$\left(\rho C_p\right)_{nf} = (1-\phi)\left(\rho C_p\right)_{bl} + \phi\left(\rho C_p\right)_{CNT} \tag{8}$$

$$k_{nf} = k_f\left(\frac{(1-\phi) + \frac{2\phi k_{CNT}}{k_{CNT}-k_f} log\left(\frac{k_{CNT}+k_f}{2k_f}\right)}{(1-\phi) + \frac{2\phi k_f}{k_{CNT}-k_f} log\left(\frac{k_{CNT}+k_f}{2k_f}\right)}\right) \tag{9}$$

where suffixes bl and CNT corresponding to the base liquid and carbon nanotubes respectively, ϕ is the volume fraction of carbon nanotubes. Table 1 shows the physical properties of the base liquids and solid nanoparticles.

Surface of the disk (at $z = 0$) is assumed to be rough and the scale of roughness is much smaller than the liquid thickness. So, the no-slip boundary condition is no longer valid on the disk surface. However, the Navier's partial slip condition may be applied to the envelop of the protuberances (see, Miklavčič and Wang (2004)) and we have boundary condition at $z = 0$ as;

$$\begin{aligned} &u = N_1\mu_{nf}\frac{\partial u}{\partial z}, \qquad v = r\Omega + N_2\mu_{nf}\frac{\partial v}{\partial z}, \\ &w = 0, \qquad T = T_0 - \frac{\gamma r^2}{2}T_1 \end{aligned} \tag{10}$$

where N_1, N_2 are the slip coefficients along the radial and azimuthal directions. T_0 and T_1 are the positive constants. Here, $\gamma > 0$ or $\gamma < 0$ represent the case of heating and cooling respectively.

At the free surface $z = h(t)$;

$$-p + 2\mu_{nf}\frac{\partial w}{\partial z} = 0 \tag{11}$$

$$\mu_{nf}\left(\frac{\partial w}{\partial r} + \frac{\partial u}{\partial z}\right) = \frac{\partial\sigma}{\partial T}\frac{\partial T}{\partial r} \tag{12}$$

$$\mu_{nf}\frac{\partial v}{\partial z} = \frac{\partial\sigma}{\partial T}\frac{\partial T}{\partial z} \tag{13}$$

$$\frac{\partial T}{\partial z} = 0 \tag{14}$$

$$\frac{dh}{dt} = w \tag{15}$$

here σ is the surface tension defined as $\sigma = \sigma_0[1 - \chi(T - T_0)]$, χ is positive constant and σ_0 is the initial surface tension.

The initial condition at t = 0 are:

$$u = v = w = 0, h = h_0, T = T_0 \tag{16}$$

Introducing the following similarity transformations (see, Dandapat and Roy (1994), Maity (2017)) as

$$\begin{aligned} &u(r,z,t) = r\overline{U}(z,t), v(r,z,t) = r\overline{V}(z,t), \\ &w(r,z,t) = \overline{W}(z,t), p = -\frac{r^2}{2}\rho\overline{A}(z,t) + \overline{B}(z,t), \\ &T(r,z,t) = T_0 - \left(\gamma\frac{r^2}{2}\right)\overline{\Theta}(z,t) - \gamma\overline{\Psi}(z,t) \end{aligned} \tag{17}$$

in the system of Eqs. (1)-(5), we found the set of Eq.s given below after comparing terms with different powers of r.

$$2\overline{U} + \frac{\partial\overline{W}}{\partial z} = 0 \tag{18}$$

$$\rho_{nf}\left[\frac{\partial\overline{U}}{\partial t} + \overline{U}^2 - \overline{V}^2 + \overline{W}\frac{\partial\overline{U}}{\partial z}\right] = \overline{A} + \mu_{nf}\frac{\partial^2\overline{U}}{\partial z^2} \tag{19}$$

$$\rho_{nf}\left[\frac{\partial\overline{V}}{\partial t} + 2\overline{U}\ \overline{V} + \overline{W}\frac{\partial\overline{V}}{\partial z}\right] = \mu_{nf}\frac{\partial^2\overline{V}}{\partial z^2} \tag{20}$$

$$\rho_{nf}\left[\frac{\partial\overline{W}}{\partial t} + \overline{W}\frac{\partial\overline{W}}{\partial z}\right] = \mu_{nf}\frac{\partial^2\overline{W}}{\partial z^2} - \frac{\partial^2\overline{B}}{\partial z^2} \tag{21}$$

$$\frac{\partial\overline{A}}{\partial z} = 0 \tag{22}$$

$$\left(\rho C_p\right)_{nf}\left[\frac{\partial\overline{\Theta}}{\partial t} + 2\,\overline{U}\,\overline{\Theta} + \overline{W}\frac{\partial\overline{\Theta}}{\partial z}\right] = k_{nf}\frac{\partial^2\overline{\Theta}}{\partial z^2} \tag{23}$$

$$\left(\rho C_p\right)_{nf}\left[\frac{\partial\overline{\Psi}}{\partial t} + \overline{W}\frac{\partial\overline{\Psi}}{\partial z}\right] = k_{nf}\left[2\overline{\Theta} + \frac{\partial^2\overline{\Psi}}{\partial z^2}\right] \tag{24}$$

The term appeared on the right side of the Eq. (23) is due to the transformation of axial thermal conductivity term in $z-$ direction of the energy Eq. (5). The first and second terms on the right side of the Eq. (24) appeared as a result of the transformation of radial thermal conductivity term in $r-$direction and axial thermal conductivity term in z-direction respectively of the energy Eq. (5) (see, Shevchuk (2022, 2023)). Due to omission of the radial thermal conductive term from the energy Eq. (5), the Eq. (23) remains unchanged whereas the Eq. (24) reduces to the Eq. (25).

$$\left(\rho C_p\right)_{nf}\left[\frac{\partial\overline{\Psi}}{\partial t} + \overline{W}\frac{\partial\overline{\Psi}}{\partial z}\right] = k_{nf}\frac{\partial^2\overline{\Psi}}{\partial z^2} \tag{25}$$

So, omission of the radial thermal conductivity along

r −direction in the energy Eq. (5) does not affect the liquid velocity and film thinning process. But this term plays an important role in film temperature distribution.

By using (17) to the boundary and initial conditions we obtain:
at $z = 0$;

$$\overline{U} = N_1\mu_{nf}\frac{\partial\overline{U}}{\partial z}, \overline{V} = \Omega + N_2\mu_{nf}\frac{\partial\overline{V}}{\partial z}, \quad \overline{W} = 0, \overline{\Theta} = T_1, \overline{\Psi} = 0 \tag{26}$$

at the surface $z = h(t)$;

$$\overline{A} = 0, \overline{B} = 2\mu_{nf}\frac{\partial\overline{W}}{\partial z} \tag{27}$$

$$\frac{\partial\overline{U}}{\partial z} = \left(\frac{\gamma\chi\sigma_0}{\mu_{nf}}\right)\overline{\Theta} \tag{28}$$

$$\frac{\partial\overline{V}}{\partial z} = 0, \frac{\partial\overline{\Theta}}{\partial z} = 0, \frac{\partial\overline{\Psi}}{\partial z} = 0 \tag{29}$$

$$\frac{dh}{dt} = \overline{W} \tag{30}$$

at $t = 0$;

$$\overline{U} = 0, \overline{V} = 0, \overline{W} = 0, h = h_0, \overline{\Theta} = 0, \overline{\Psi} = 0 \tag{31}$$

Now introducing the following dimensionless variables given in (32) into the above system of Eqs. (18)-(20) and (23)-(24).

$$\tau = t/t_c, \quad \xi = \frac{z}{h_0}, \quad H = \frac{h}{h_0}, \quad U = \frac{\overline{U}h_0}{U_0}, \quad V = \frac{\overline{V}}{\Omega}, \quad W = \frac{\overline{W}}{U_0}, \quad \Theta = \frac{h_0^2\overline{\Theta}}{\Delta T}, \quad \Psi = \frac{\overline{\Psi}}{\Delta T} \tag{32}$$

where t_c and $U_0 = h_0/t_c$ are the characteristic time and characteristic velocity respectively, $\Delta T = |\gamma h_0^2 T_1|$. The non-dimensional form of the Eqs. (18)-(20) and (23)-(24) are given below.

$$2U + \frac{\partial W}{\partial\xi} = 0 \tag{33}$$

$$Re\phi_1\left(\frac{\partial U}{\partial\tau} + U^2 + W\frac{\partial U}{\partial\xi}\right) = \frac{\partial^2 U}{\partial\xi^2} + \phi_1 V^2 \tag{34}$$

$$Re\phi_1\left(\frac{\partial V}{\partial\tau} + 2UV + W\frac{\partial V}{\partial\xi}\right) = \frac{\partial^2 V}{\partial\xi^2} \tag{35}$$

$$RePr\phi_2\left(\frac{\partial\Theta}{\partial\tau} + 2U\Theta + W\frac{\partial\Theta}{\partial\xi}\right) = \frac{k_{nf}}{k_f}\frac{\partial^2\Theta}{\partial\xi^2} \tag{36}$$

$$RePr\phi_2\left(\frac{\partial\Psi}{\partial\tau} + W\frac{\partial\Psi}{\partial\xi}\right) = \frac{k_{nf}}{k_f}\left(2\Theta + \frac{\partial^2\Psi}{\partial\xi^2}\right) \tag{37}$$

where $Re = \frac{\Omega h_0^2}{\nu_f}$, $Pr = \frac{\nu_f}{\alpha_f}$, $\alpha_f = \frac{k_f}{\rho C_{p_f}}$, ν_f are the Reynolds number, Prandtl number, thermal diffusivity and kinematic viscosity of the base liquid respectively and $\phi_1 = (1-\phi)^{\frac{5}{2}}\left[(1-\phi) + \phi\frac{\rho_s}{\rho_f}\right]$, $\phi_2 = \left[(1-\phi) + \phi\frac{(\rho C_p)_s}{(\rho C_p)_f}\right]$ are dimensionless constants.

The non-dimensional form of the Eq. (25) is given by Eq. (38).

$$RePr\phi_2\left(\frac{\partial\Psi}{\partial\tau} + W\frac{\partial\Psi}{\partial\xi}\right) = \frac{k_{nf}}{k_f}\frac{\partial^2\Psi}{\partial\xi^2} \tag{38}$$

The dimensionless boundary conditions are given by the Eqs. (39) and (40).

At $\xi = 0$,

$$U = \lambda(1-\phi)^{\frac{-5}{2}}U_\xi, \quad V = 1 + \delta(1-\phi)^{\frac{-5}{2}}V_\xi, \quad W = 0, \quad \Theta = 1, \quad \Psi = 0 \tag{39}$$

where $\lambda = \frac{N_1\mu_f}{h_0}$ and $\delta = \frac{N_2\mu_f}{h_0}$ are the roughness parameter along the radial and azimuthal directions respectively.

At $\xi = H(\tau)$

$$U_\xi = \gamma\alpha(1-\phi)^{\frac{5}{2}}\Theta, \quad V_\xi = 0, \quad \Theta_\xi = 0, \quad \Psi_\xi = 0, \quad \frac{dH}{d\tau} = W \tag{40}$$

where $\alpha = \chi\sigma_0\Delta T/\Omega h_0\mu_f$ is the thermocapillary parameter.

Now dimensionless initial conditions are given in the Eq. (41).

$$U = V = W = 0, \Theta = \Psi = 0, H(0) = 1 \tag{41}$$

It is to be pointed out here that, the above non-dimensional governing Eqs. (33)-(37) and associated conditions (39)-(41) matches with that of the non-dimensional equations and conditions obtained by Dandapat and Roy (1994) in case of pure liquid and no roughness (i.e., ϕ= 0, λ = 0 and δ = 0).

3. Analytical solution

The analytical solutions for coupled non-linear system of Eqs. (33)-(41) are computed under assumption that the Reynolds number $Re(\ll 1)$ is small. All the dependent variables are expanded by the asymptotic procedure (42).

$$(U, V, W, \Theta, \Psi) = (U_0, V_0, W_0, \Theta_0, \Psi_0) + Re(U_1, V_1, W_1, \Theta_1, \Psi_1) + O(Re^2) \tag{42}$$

The Eq. (42) is substituted in (33)-(41) and comparing the coefficients of like power of *Re* from both sides, one can obtain the set of equations involving dependent variables *U*, *V*, *W*, Θ and Ψ. These equations are solved up to *O*(*Re*) and the following expressions are obtained.

$$U = \phi_1\left(H\xi - \frac{\xi^2}{2}\right) + \alpha\gamma(1-\phi)^{5/2}\xi + \lambda\phi_1 H(1-\phi)^{-5/2} + \lambda\alpha\gamma + Re\phi_1\left[\frac{\phi_1 H'}{2}\left(\frac{\xi^3}{3} - H^2\xi\right) + \lambda\phi_1(1-\phi)^{-5/2}H'\left(\frac{\xi^2}{2} - H\xi\right) + \phi_1^2\left(\frac{\xi^6}{360} - \frac{H\xi^5}{60} + \frac{2}{9}H^3\xi^3 - \frac{9}{15}H^5\xi\right) + \phi_1\alpha\gamma(1-\phi)^{5/2}\left(\frac{H^2\xi^3}{3} - H^4\xi\right) + \lambda\phi_1^2(1-\phi)^{-5/2}\left(\frac{2}{3}H^2\xi^3 - \frac{1}{12}H\xi^4 - \frac{11}{3}H^4\xi\right) + \lambda\phi_1\alpha\gamma\left(\frac{2}{3}H\xi^3 - \frac{1}{12}\xi^4 - \frac{5}{3}H^3\xi\right) + \lambda^2\phi_1^2(1-\phi)^{-5}H^2\left(\frac{\xi^2}{2} - H\xi\right) + \lambda^2\alpha^2\gamma^2\left(\frac{\xi^2}{2} - H\xi\right) + 2\lambda^2\alpha\phi_1\gamma(1-\phi)^{-5/2}\left(\frac{H\xi^2}{2} - H^2\xi\right) + 2\delta A(H)\left(\frac{\xi^2}{2} - H\xi\right)\right] + ReB(H)\xi + ReC(H) \tag{43}$$

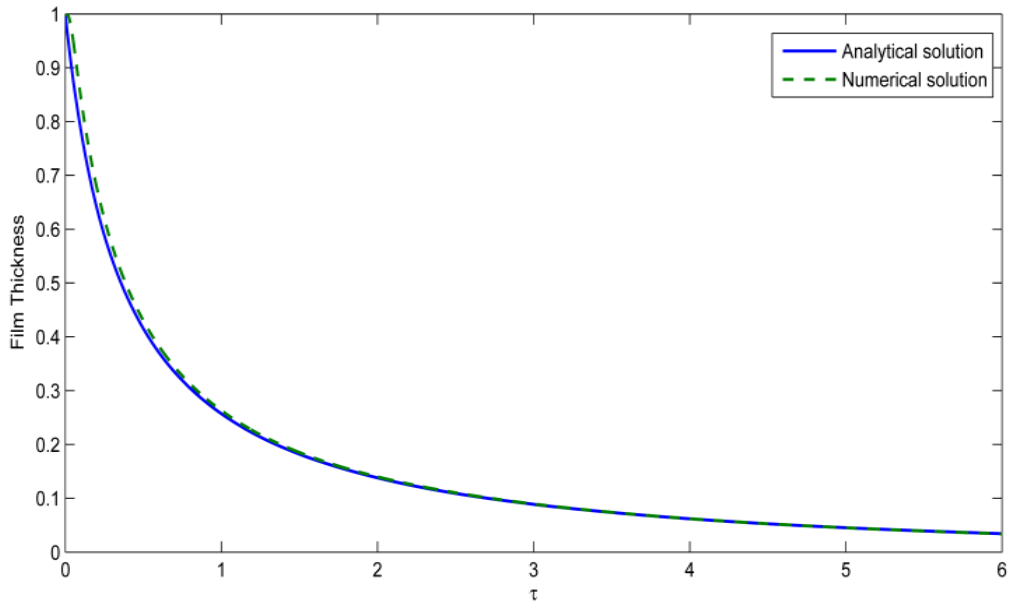

Fig. 2 Here, Re = 0.01, λ = 1.0, δ = 1.0, α = 0.1, γ = 1 and $\phi = 0.01$. Solid line for analytical solution and dashed line for numerical solution

$$V = 1 + Re\left[2\phi_1^2\left(\frac{H\xi^3}{6} - \frac{\xi^4}{24} - \frac{H^3\xi}{3}\right) + 2\phi_1\alpha\gamma(1-\phi)^{5/2}\left(\frac{\xi^3}{6} - \frac{H^2\xi}{2}\right) + 2\phi_1^2\lambda H(1-\phi)^{-5/2}\left(\frac{\xi^2}{2} - H\xi\right) + 2\phi_1\lambda\alpha\gamma\left(\frac{\xi^2}{2} - H\xi\right) - A(H)\delta\right] \quad (44)$$

$$W = -2\phi_1\left(\frac{H\xi^2}{2} - \frac{\xi^3}{6}\right) - \alpha\gamma(1-\phi)^{5/2}\xi^2 - 2\lambda\phi_1 H(1-\phi)^{-5/2}\xi - 2\lambda\alpha\gamma\xi - 2Re\phi_1\left[\frac{\phi_1 H'}{2}\left(\frac{\xi^4}{12} - \frac{H^2\xi^2}{2}\right) + \lambda\phi_1(1-\phi)^{-5/2}H'\left(\frac{\xi^3}{6} - \frac{H\xi^2}{2}\right) + \phi_1^2\left(\frac{\xi^7}{2520} - \frac{H\xi^6}{360} + \frac{1}{18}H^3\xi^4 - \frac{3}{10}H^5\xi^2\right) + \phi_1\alpha\gamma(1-\phi)^{5/2}\left(\frac{H^2\xi^4}{12} - \frac{H^4\xi^2}{2}\right) + \lambda\phi_1^2(1-\phi)^{-5/2}\left(\frac{H^2\xi^4}{6} - \frac{H\xi^5}{60} - \frac{11}{6}H^4\xi^2\right) + \lambda\phi_1\alpha\gamma\left(\frac{1}{6}H\xi^4 - \frac{1}{60}\xi^5 - \frac{5}{6}H^3\xi^2\right) + \lambda^2\phi_1^2(1-\phi)^{-5}H^2\left(\frac{\xi^3}{6} - \frac{H\xi^2}{2}\right) + \lambda^2\alpha^2\gamma^2\left(\frac{\xi^3}{6} - \frac{H\xi^2}{2}\right) + 2\lambda^2\alpha\phi_1\gamma(1-\phi)^{-5/2}\left(\frac{H\xi^3}{6} - \frac{H^2\xi^2}{2}\right) + 2\delta A(H)\left(\frac{\xi^3}{6} - \frac{H\xi^2}{2}\right)\right] - Re(B(H)\xi^2 + 2C(H)\xi) \quad (45)$$

$$\Theta = 1 + \frac{2RePr\phi_2}{K}\left[\phi_1\left(\frac{H\xi^3}{6} - \frac{\xi^4}{24} - \frac{H^3\xi}{3}\right) + \frac{1}{2}\alpha\gamma(1-\phi)^{5/2}\left(\frac{\xi^3}{3} - H^2\xi\right) + \lambda\phi_1 H(1-\phi)^{-5/2}\left(\frac{\xi^2}{2} - H\xi\right) + \lambda\alpha\gamma\left(\frac{\xi^2}{2} - H\xi\right)\right] \quad (46)$$

$$\Psi = 2\left(H\xi - \frac{\xi^2}{2}\right) + \frac{2RePr\phi_2}{K}\left[\frac{H'}{2}\left(\frac{\xi^3}{3} - H^2\xi\right) - 2\phi_1\left(\frac{\xi^6}{240} - \frac{H\xi^5}{40} + \frac{H^2\xi^4}{24} - \frac{H^3\xi^3}{18} + \frac{H^5\xi}{10}\right) + \alpha\gamma(1-\phi)^{5/2}\left(\frac{\xi^5}{30} - \frac{H\xi^4}{12} + \frac{H^2\xi^3}{6} - \frac{H^4\xi}{3}\right) + \frac{1}{3}\lambda\phi_1 H(1-\phi)^{-5/2}\left(\frac{\xi^4}{4} - H^3\xi\right) + \frac{1}{3}\lambda\alpha\gamma\left(\frac{\xi^4}{4} - H^3\xi\right)\right] \quad (47)$$

where

$$A(H) = \frac{2}{3}\phi_1^2 H^3(1-\phi)^{-5/2} + \phi_1\alpha\gamma H^2 + 2\phi_1^2\lambda(1-\phi)^{-5}H^2 + 2\phi_1\lambda\alpha\gamma(1-\phi)^{-5/2}H,$$

$$B(H) = \frac{2Pr\phi_2\gamma\alpha}{K}(1-\phi)^{5/2}\left[-\frac{5}{24}\phi_1 H^4 - \frac{1}{3}\alpha\gamma(1-\phi)^{5/2}H^3 - \frac{1}{2}\lambda\phi_1(1-\phi)^{-5/2}H^3 - \frac{1}{2}\lambda\alpha\gamma H^2\right],$$

$$C(H) = \lambda(1-\phi)^{-5/2}\left[\phi_1\left(-\frac{\phi_1 H'}{2}H^2 - \lambda\phi_1(1-\phi)^{-5/2}HH' + \phi_1^2\left(-\frac{9}{15}H^5\right) + \phi_1\alpha\gamma(1-\phi)^{5/2}(-H^4) + \lambda\phi_1^2(1-\phi)^{-5/2}\left(-\frac{11}{3}H^4\right) + \lambda\phi_1\alpha\gamma\left(-\frac{5}{3}H^3\right) + \lambda^2\phi_1^2(1-\phi)^{-5}(-H^3) + \lambda^2\alpha^2\gamma^2(-H) + 2\lambda^2\alpha\phi_1\gamma(1-\phi)^{-5/2}(-H^2) + 2\delta A(H)(-H)\right) + B(H)\right]$$ and $K = \frac{k_{nf}}{k_f}$.

The evolution equations for transient film thickness $H(\tau)$ is derived upon substitution of expression for W in (40). The film evolution equations accurate up to $O(Re)$ is given in (48).

$$\frac{dH}{d\tau} = -\frac{2}{3}\phi_1 H^3 - \alpha\gamma(1-\phi)^{5/2}H^2 - 2\lambda\phi_1(1-\phi)^{-5/2}H^2 - 2\lambda\alpha\gamma H + Re\left[\frac{5}{12}\phi_1^2 H'H^4 + \frac{1}{3}\lambda\phi_1^2(1-\phi)^{-5/2}H'H^3 + \phi_1^3\frac{311}{630}H^7 + \frac{5}{6}\phi_1^2\alpha\gamma(1-\phi)^{5/2}H^6 + \frac{101}{30}\lambda\phi_1^3(1-\phi)^{-5/2}H^6 + \frac{41}{30}\lambda\phi_1^2\alpha\gamma H^5 + \frac{2}{3}\lambda^2\phi_1^3(1-\phi)^{-5}H^5 + \frac{2}{3}\phi_1\lambda^2\alpha^2\gamma^2H^3 + \frac{4}{3}\phi_1^2\lambda^2\alpha\gamma(1-\phi)^{-5/2}H^4 + \frac{4}{3}\phi_1\delta A(H)H^3 - B(H)H^2 - 2C(H)H\right] \quad (48)$$

To solve the evolution Eq. (48), the film thickness $H(\tau)$ is expanded in power of *Re* as per Eq. (49).

$$H(\tau) = H_0(\tau) + ReH_1(\tau) + O(Re^2) \quad (49)$$

Substituting the Eq. (49) in (48) and equating the coefficients of like order *Re* from both the sides, one may

Table 2 Comparison of present solutions with the analytical solutions of Dandapat and Roy (1994) for *Re* = 0.01, *Pr* = 0.5, α = 0.5 and γ = 1, φ = 0, λ = 0 and δ = 0

Time (τ)	Film thickness $h(\tau)$	
	Dandapat and Roy (1994)	Present Solution
0.0	1.00000	1.00000
0.2	0.82023	0.82024
0.4	0.70435	0.70432
0.6	0.62207	0.62201
0.8	0.55995	0.55986
1.0	0.51100	0.51090
1.5	0.42352	0.42340
2.0	0.36474	0.36463
2.5	0.32201	0.32190
3.0	0.28927	0.28917
3.5	0.26325	0.26315
4.0	0.24198	0.24189
4.5	0.22421	0.22413
5.0	0.20911	0.20904

obtain Eq. (50) at the leading order of *Re*

$$\frac{dH_0}{d\tau} = -\frac{2}{3}\phi_1 H_0^3 - \alpha\gamma(1-\phi)^{5/2}H_0^2 - 2\lambda\phi_1(1-\phi)^{-5/2}H_0^2 - 2\lambda\alpha\gamma H_0 \tag{50}$$

whereas, at the first order of *Re* one can get the Eq. (51).

$$\begin{aligned}\frac{dH_1}{d\tau} &= -2\phi_1 H_0^2 H_1 - 2\alpha\gamma(1-\phi)^{5/2}H_0 H_1 \\ &-4\lambda\phi_1(1-\phi)^{-5/2}H_0 H_1 - 4\lambda\alpha\gamma H_0 H_1 + \frac{5}{12}\phi_1^2 H_0' H_0^4 \\ &+\frac{1}{3}\lambda\phi_1^2(1-\phi)^{-5/2}H_0' H_0^3 + \phi_1^3\frac{311}{630}H_0^7 \\ &+\frac{5}{6}\phi_1^2\alpha\gamma(1-\phi)^{5/2}H_0^6 + \frac{101}{30}\lambda\phi_1^3(1-\phi)^{-5/2}H_0^6 \\ &+\frac{41}{30}\lambda\phi_1^2\alpha\gamma H_0^5 + \frac{2}{3}\lambda^2\phi_1^3(1-\phi)^{-5}H_0^5 \\ &+\frac{2}{3}\phi_1\lambda^2\alpha^2\gamma^2 H_0^3 + \frac{4}{3}\phi_1^2\lambda^2\alpha\gamma(1-\phi)^{-5/2}H_0^4 \\ &+\frac{4}{3}\phi_1\delta A(H_0)H_0^3 - B(H_0)H_0^2 - 2C(H_0)H_0\end{aligned} \tag{51}$$

The Eqs. (50) and (51) are solved numerically by using Runge-Kutta method with the initial conditions $H_0(0) = 1$ and $H_1(0) = 0$.

4. Numerical solution

The numerical solution of non-linear system of PDE's (33)-(37) are obtained by the implicit finite difference technique. In our model $H(\tau)$ is continuously reduced with τ, as a result the physical domain [0, $H(\tau)$] always changes with time. To apply the finite difference technique, one need to transfer the time varying physical domain to a fixed computational domain. The transformation (52) is considered to transfer the physical domain to a constant domain (see, Robert (1971)) in which film thickness $H(\tau) \in [0,1]$.

$$\eta(\tau) = 1 - \alpha_1 ln\left(\frac{\alpha_2 H(\tau) - \xi}{\beta_1 H(\tau) + \xi}\right) \tag{52}$$

where $\alpha_1 = [ln(\alpha_2/\beta_1)]^{-1}$, $\alpha_2 = \beta + 1$ and $\beta_1 = \beta - 1$. $\beta(1 < \beta < \infty)$ is grid spacing parameter (small β gives the cluster grid distribution near disk but large β build uniform grid distribution throughout the nanoliquid film). By using transformation (52) the Eqs. (33)-(37) are transformed then solved by the Crank-Nicholson scheme and the nonlinear terms are linearized by Newton's linearization technique. Finally, the numerical computations are carried out with the tridiagonal system of algebraic Eqs. given by the Eqs. (53)-(56).

$$PU_{j-1}^{n+1} + QU_j^{n+1} + RU_{j+1}^{n+1} = (S_1)_j^n \tag{53}$$

$$PV_{j-1}^{n+1} + QV_j^{n+1} + RV_{j+1}^{n+1} = (S_2)_j^n \tag{54}$$

$$P_1\Theta_{j-1}^{n+1} + Q_1\Theta_j^{n+1} + R_1\Theta_{j+1}^{n+1} = (S_3)_j^n \tag{55}$$

$$P_1\Psi_{j-1}^{n+1} + Q_1\Psi_j^{n+1} + R_1\Psi_{j+1}^{n+1} = (S_4)_j^n \tag{56}$$

where

$$P = \frac{B_1 - A_1}{4\Delta\eta} - \frac{C}{2(\Delta\eta)^2}, \quad Q = \frac{1}{\Delta\tau} + \frac{C}{(\Delta\eta)^2} + 2U_j^n, \quad R = \frac{A_1 - B_1}{4\Delta\eta} - \frac{C}{2(\Delta\eta)^2} \tag{57}$$

$$(S_1)_j^n = U_{j-1}^n\left[\frac{A_1-B_1}{4\Delta\eta} + \frac{C}{2(\Delta\eta)^2}\right] + U_j^n\left[\frac{1}{\Delta\tau} - \frac{C}{(\Delta\eta)^2} + U_j^n\right] + U_{j+1}^n\left[\frac{B_1-A_1}{4\Delta\eta} + \frac{C}{2(\Delta\eta)^2}\right] + \frac{1}{Re\phi_1}\left(V_j^n\right)^2 \tag{58}$$

$$(S_2)_j^n = V_{j-1}^n\left[\frac{A_1 - B_1}{4\Delta\eta} + \frac{C}{2(\Delta\eta)^2}\right] + V_j^n\left[\frac{1}{\Delta\tau} - \frac{C}{(\Delta\eta)^2}\right] + V_{j+1}^n\left[\frac{B_1 - A_1}{4\Delta\eta} + \frac{C}{2(\Delta\eta)^2}\right] \tag{59}$$

$$P_1 = \frac{D - A_1}{4\Delta\eta} - \frac{E}{2(\Delta\eta)^2}, Q_1 = \frac{1}{\Delta\tau} + \frac{E}{(\Delta\eta)^2}, \quad R_1 = \frac{A_1 - D}{4\Delta\eta} - \frac{E}{2(\Delta\eta)^2} \tag{60}$$

$$(S_3)_j^n = \Theta_{j-1}^n\left[\frac{A_1 - D}{4\Delta\eta} + \frac{E}{2(\Delta\eta)^2}\right] + \Theta_j^n\left[\frac{1}{\Delta\tau} - 2U_j^n - \frac{E}{(\Delta\eta)^2}\right] + \Theta_{j+1}^n\left[\frac{D - A_1}{4\Delta\eta} + \frac{E}{2(\Delta\eta)^2}\right] \tag{61}$$

$$(S_4)_j^n = \Psi_{j-1}^n\left[\frac{A_1-D}{4\Delta\eta} + \frac{E}{2(\Delta\eta)^2}\right] + \Psi_j^n\left[\frac{1}{\Delta\tau} - 2U_j^n - \frac{E}{(\Delta\eta)^2}\right] + \Psi_{j+1}^n\left[\frac{D-A_1}{4\Delta\eta} + \frac{E}{2(\Delta\eta)^2}\right] + \frac{2}{RePr\phi_2}\left(\frac{k_{nf}}{k_f}\right)\Theta_j^n \tag{62}$$

$$A_1 = \frac{\alpha_1(\alpha_2 + \beta_1)\big(WH(\tau) - \xi H'(\tau)\big)}{(\alpha_2 H(\tau) - \xi)(\beta_1 H(\tau) + \xi)} \tag{63}$$

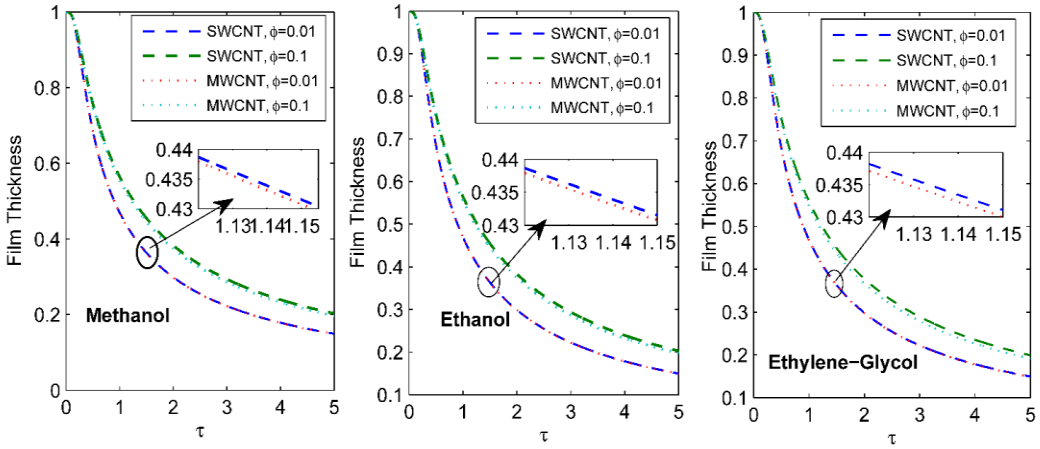

(a) (b) (c)

Fig. 3 Here, Re = 0.1, λ = 0.5, δ = 0.5, α = 1.0, γ = −1 where (a) for methanol, (b) for ethanol, and (c) for ethylene-glycol

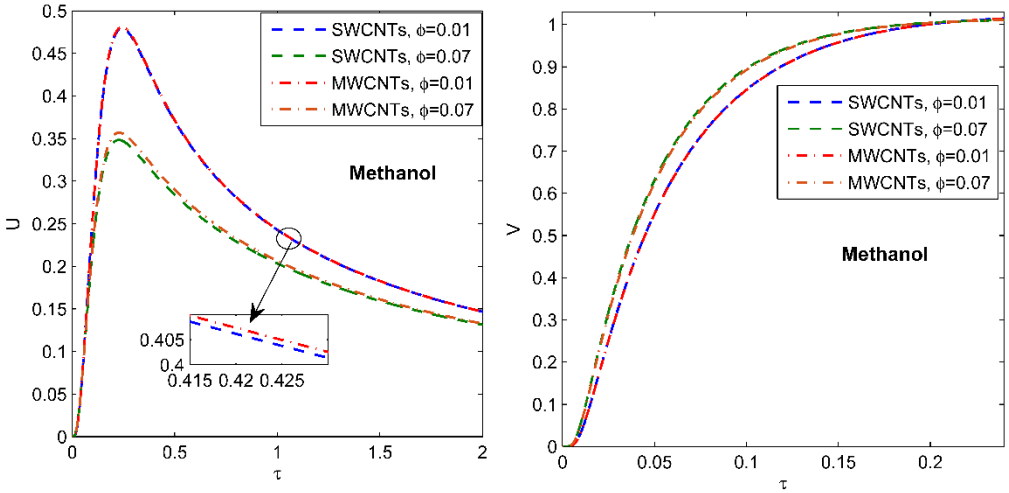

(a) (b)

Fig. 4 Here, Re = 0.1, λ = 0.1, α = 1.0, δ = 0.1, γ = −1, Z = H

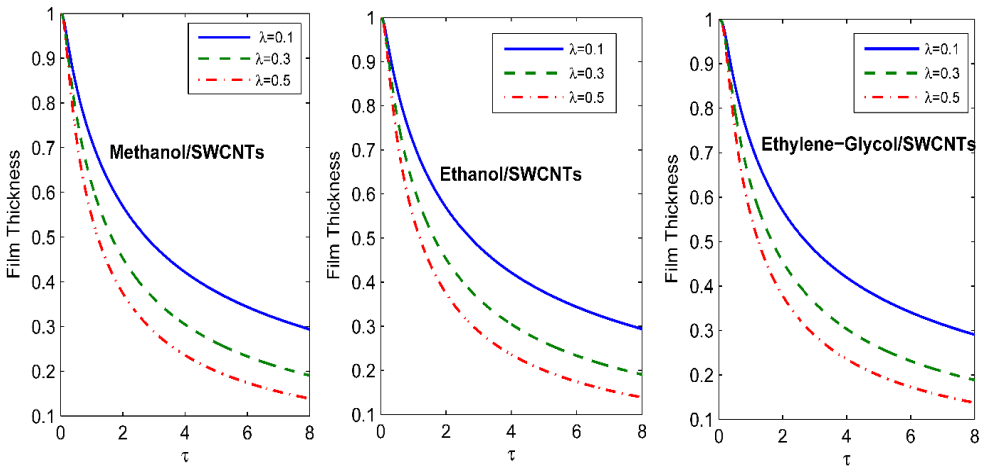

(a) (b) (c)

Fig. 5 Here, *Re* = 0.1, ϕ = 0.1, δ = 0.1, α = 1.0, γ = −1 where (a) for methanol, (b) for ethanol, and (c) for ethylene-glycol

$$B_1 = \frac{1}{Re\phi_1}\left[\frac{\alpha_1(\alpha_2+\beta_1)H(\tau)[(\beta_1-\alpha_2)H(\tau)+2\xi]}{(\alpha_2 H(\tau)-\xi)^2(\beta_1 H(\tau)+\xi)^2}\right] \quad (64)$$

$$C = \frac{1}{Re\phi_1}\left[\frac{\alpha_1(\alpha_2+\beta_1)H(\tau)}{(\alpha_2 H(\tau)-\xi)(\beta_1 H(\tau)+\xi)}\right]^2 \quad (65)$$

$$D = \frac{1}{RePr\phi_2}\left(\frac{k_nf}{k_f}\right)\times\left[\frac{\alpha_1(\alpha_2+\beta_1)H(\tau)[(\beta_1-\alpha_2)H(\tau)+2\xi]}{(\alpha_2 H(\tau)-\xi)^2(\beta_1 H(\tau)+\xi)^2}\right] \quad (66)$$

$$E = \frac{1}{RePr\phi_2}\left(\frac{k_nf}{k_f}\right)\left[\frac{\alpha_1(\alpha_2+\beta_1)H(\tau)}{(\alpha_2 H(\tau)-\xi)(\beta_1 H(\tau)+\xi)}\right]^2 \quad (67)$$

At a fixed time, level U, V, Θ and Ψ are computed from the above tridiagonal system of Eqs. (53)-(56). Hence, W and H are computed from the Eq. of continuity and kinematic condition respectively.

The computation of the variables U, V, W, Θ, Ψ and H are continued until satisfying the following convergence criterion:

$$\frac{\sum_j\left|\Pi_j^{n+1}-\Pi_j^n\right|}{\sum_j\left|\Pi_j^{n+1}\right|} \le \epsilon \quad (68)$$

where $\prod$ = (U, V, W, Θ, Ψ, H), ε is the convergence criterium which is taken as $\varepsilon = 10^{-6}$.

The numerical simulations are done with 51 grid points along vertical direction with $\beta = 10^4$ and this provides the uniform grid distribution in computational domain. The time step for numerical computation is taken as

$$\delta\tau \le 0.25 \times \delta\eta^2 \quad (69)$$

which comes from the Courant-Friedrichs-Lewy (CFL) condition of numerical stability. As we have obtained the analytical solution of the flow problem for small Reynolds number (Re), in Fig. 2 a comparison between analytical and numerical solutions are made for small Re with methanol based SWCNTs nanoliquid. The figure shows that both the solutions match satisfactorily at large time. Also, we have compared the present solution with analytical solution obtained by Dandapat and Roy (1994) in Table 2 and found a very good agreement between them.

5. Results and discussions

In this article, we have investigated the effects of partial slip between liquid and disk on the flow of thin CNTs nanoliquid over a horizontal rough rotating disk. During the coating of the substrates, one has to place the substrates over the disk either arranged in concentric rings or may be placed radially symmetric or mixed of these two (see, Fig. 1). This placement of substrates over the disk leads to the roughness over the surface. The characteristics scale of the roughness is assumed to be small in compare to the film thickness. The effects of CNTs volume fraction ϕ on the film thickness has been shown in Fig. 3 for the base liquid methanol, ethanol and ethylene-glycol. It is evident from the figure that film thinning rate diminishes with the higher values of ϕ. From Eq. (7) it is clearly visible that the effective viscosity μ_{nf} increases with the increase in values of ϕ. Therefore, the rising viscosity produces more resistance on the liquid motion along radial direction. As a result, film thinning process slows down for higher values of ϕ. From Fig. 3 it is also observed that the film height reduces for the MWCNTs in comparison to SWCNTs. This is due to fact that the density of SWCNTs is higher than that of MWCNTs. The above observation may be confirmed through the velocity plot in Fig. 4. The Fig. 4 depicts the influence of volume fraction ϕ on the variation of U and V for methanol based CNTs nanoliquid. It is seen that both U and V diminishes for higher values of ϕ. The influence of radial roughness parameter λ with methanol, ethanol and ethylene-glycol based SWCNTs nanoliquids has been plotted in Fig. 5. It is found that the film thins faster for increasing values of λ for CNTs nanoliquids. In other words, roughness aligned symmetrically along the radial direction enhances film thinning. Due to the rotation of the disk, the nanoliquid which was deposited over the surface of the disk starts flowing out along the radial outward direction due to the action of the centrifugal force. This radial outward flow enhances for partial slip velocity along the radial direction. These phenomenon results in increase in the film thinning for roughness that are aligned symmetrically along the radial direction. The influence of azimuthal roughness parameter δ on the film thickness H has been explored in Fig. 6 for methanol, ethanol and ethylene-glycol based SWCNTs nanoliquids. It is seen that the symmetrical roughness aligned along the azimuthal direction resists film thinning. As a result, film thickens when the value of δ increases. The above film thinning behaviour can be clearly understood from the velocity plots in Fig. 7 for different roughness parameters. Fig. 7 shows the change of U and V with time for different values of λ and δ in methanol based CNTs nanoliquid. It is obvious from the figure that when the radial roughness parameter λ increases, the velocity components U and V also increases but opposite results are seen for increasing values of δ. Fig. 8 represents the change of film thickness H for different values of thermocapillary parameter α for methanol, ethanol and ethylene-glycol based SWCNTs nanoliquids in case of cooling (i.e. $\gamma = 1$). It is seen from the figure that, the film thinning rate increases with the increase in values of α. Here, α represents the change of surface tension with the temperature. The surface of the disk is cooling along the radial direction so the temperature at the center of the disk is maximum. The temperature gradually decreases along the radial direction. Therefore, the surface tension is minimum at the center of the disk and increases along the radial direction. As a result, a thermocapillary flow is generated from lower to higher surface tension zone at the film surface. This thermocapillary flow acts along the radial outward direction. For this reason, the film thinning rate increases with increase in values of α. One may expect the opposite result in case heating of the disk.

The dimensionless temperature profile within the nano-liquid film due to heating or cooling of the disk is dereived as

$$T = -\gamma\left(\frac{R^2}{2}\Theta + \Psi\right) \quad (70)$$

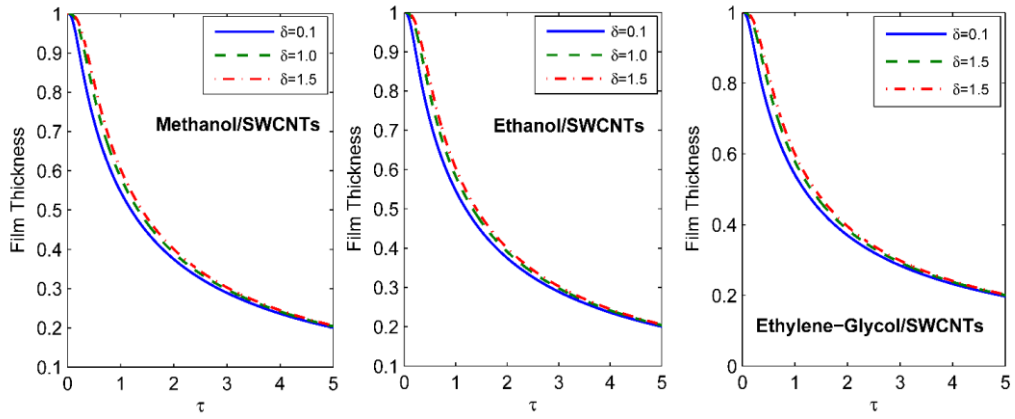

(a) (b) (c)

Fig. 6 Here, Re = 0.1, ϕ = 0.1, λ = 0.5, α = 1.0, γ = −1 where (a) for methanol, (b) for ethanol, and (c) for ethylene-glycol

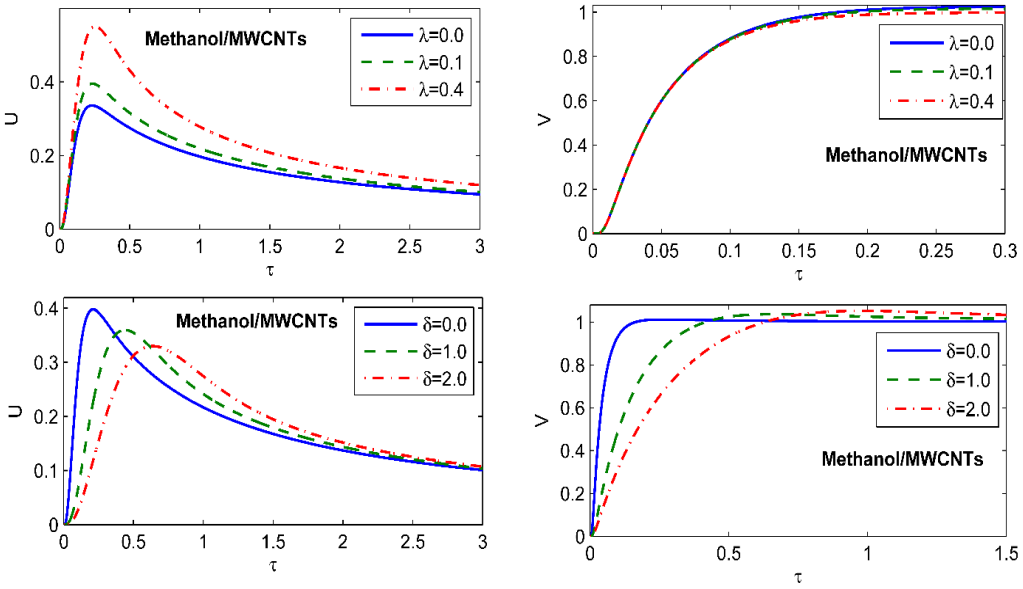

(a) (b)

Fig. 7 Here, Re = 0.1, α = 1.0, γ = −1, z = H, (a) for and δ = 0.1, (b) for λ = 0.1

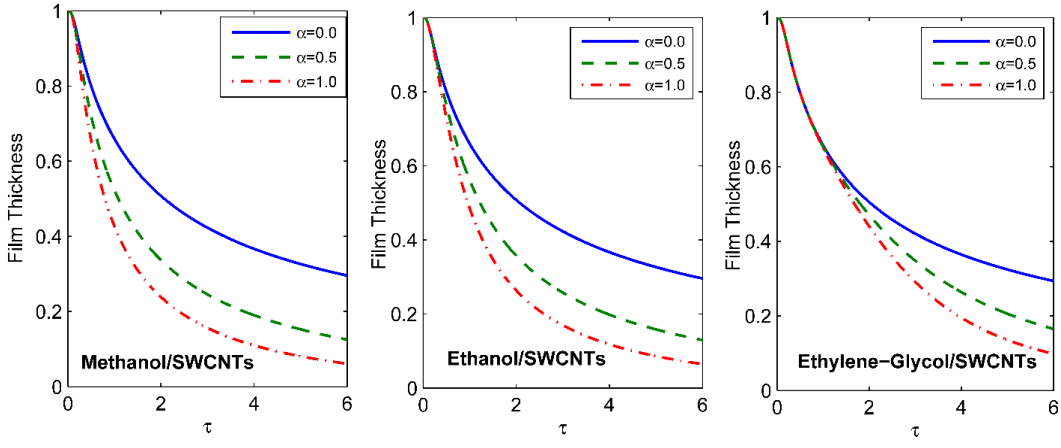

(a) (b) (c)

Fig. 8 Here, Re = 0.1, ϕ = 0.05, λ = 0.1, δ = 0.1, γ = 1 where (a) for methanol, (b) for ethanol, and (c) for ethylene-glycol

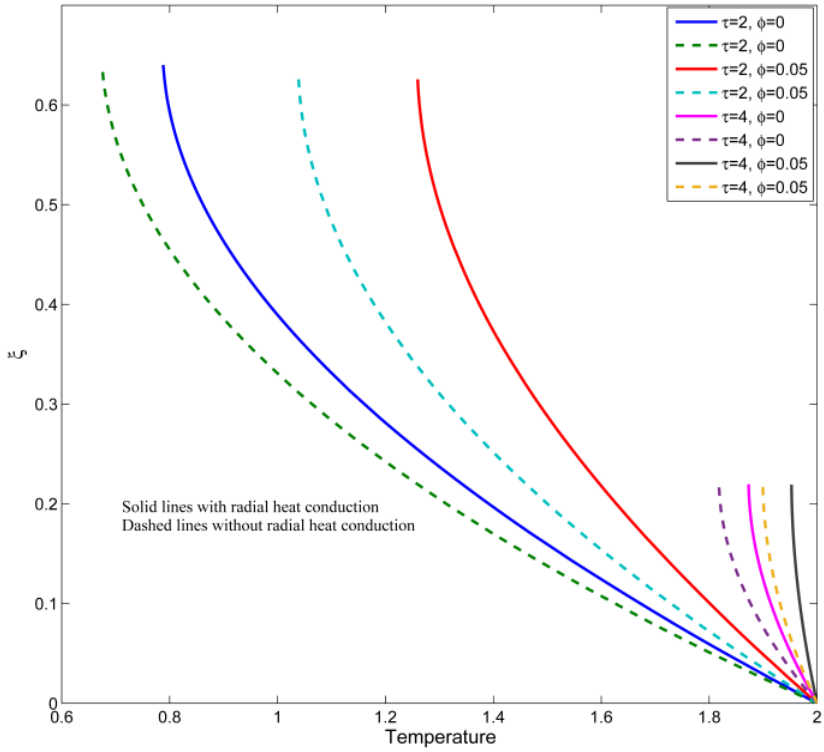

Fig. 9 Variation of film temperature along the vertical direction at different time step. Here, Re = 1.0, Pr = 7.24, λ = 1.0, δ = 1.0, α = 0.5, γ = −1

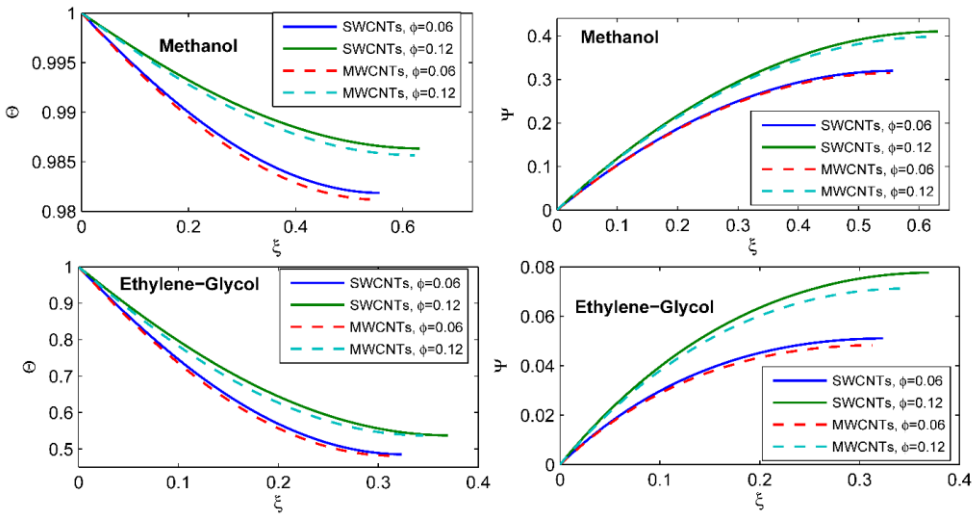

(a) (b)

Fig. 10 Here, Re = 0.1, α = 0.5, λ = 0.1, δ = 1, γ = −1 and τ = 1.8

where, $R = r/h_0$. It is obvious from the Eq. (70) that the non-dimensional temperature T depends on both Θ and Ψ. Θ is computed from the Eq. (36). Computations of Ψ were performed using Eq. (37) when considering the radial thermal conductivity term and from Eq. (38) for disregarding the radial thermal conductivity term. In Fig. 9, we have plotted the non-dimensional temperature distribution T for different values of τ and ϕ. Solid lines represents allowance of the radial heat conduction and dashed lines for disregarding of the radial heat conduction. It is observed from the figure that the temperature of liquid film increases significantly in presence of the radial heat conduction. It is also seen from the figure that in presence of nanoparticles the contribution of radial heat conduction term is more. As time increases the temperature of the liquid film also increases and it tends to disk temperature at large time. So, the contribution of the radial thermal conductive term is not negligible in this problem. In rest of the figures the radial thermal conductive term is utilized.

Fig. 10 exhibits the effects of volume fraction ϕ on the temperature profile T for methanol and ethylene-glycol based SWCNTs and MWCNTs nanoliquids when the disk is

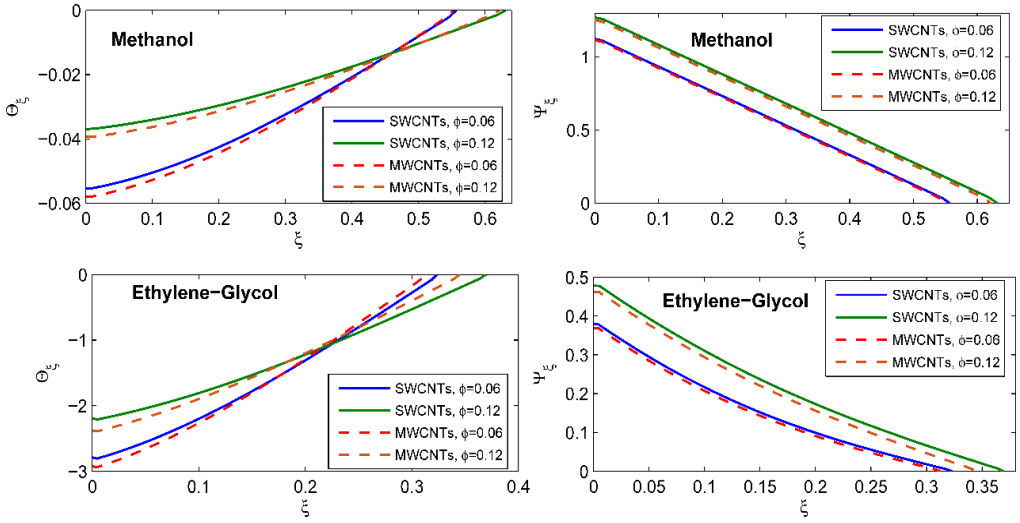

(a) (b)

Fig. 11 Here, Re = 0.1, α = 0.5, λ = 0.1, δ = 1, γ = −1 and τ = 1.8

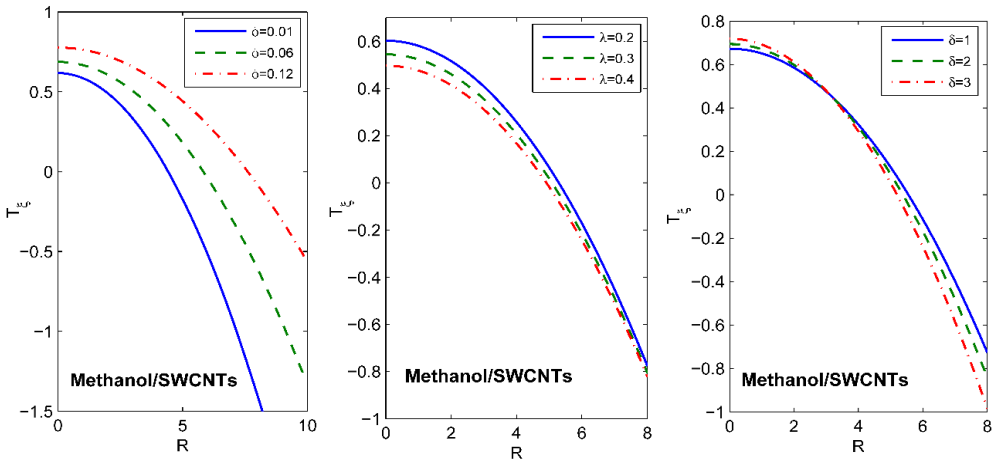

(a) (b) (c)

Fig. 12 Here, Re = 0.1, α = 1.0, γ = −1 and τ = 1.8 at ξ = 0.4H(τ). (a) for different values ϕ with λ = 0.1, δ = 1, (b) for different values of λ with ϕ = 0.05, δ = 1 and (c) for different values of δ with ϕ = 0.05, λ = 0.1

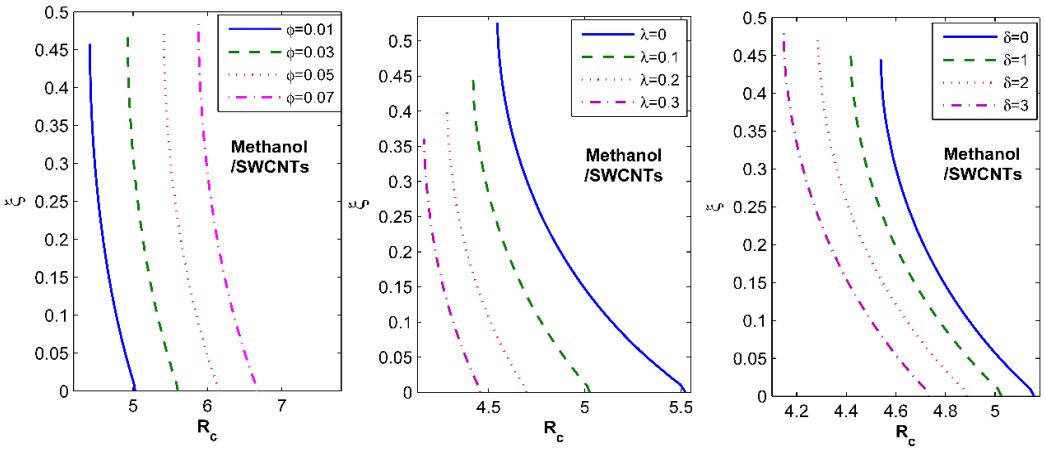

(a) (b) (c)

Fig. 13 Here, Re = 0.1, γ = −1 and τ = 2.0. (a) for different values ϕ with λ = 0.1, δ = 1 and α = 1, (b) for different values of λ with ϕ= 0.05, δ = 1 and (c) for different values of δ with ϕ = 0.05, λ = 0.1

heating (i.e., $\gamma = -1$). It is clear from the figure that Θ and Ψ increases with the higher values of ϕ at a particular height of the film. This happens as the thermal conductivity of both the nanoliquids increases with rising values of ϕ. It is also noted that both Θ and Ψ have higher values for SWCNTs in comparison with MWCTNs. Physically, the above phenomena occur, as the thermal conductivity of the SWCNTs is much more than that of the MWCNTs. Here, Θ has the decreasing nature along the thickness of CNTs nanoliquid film for a fixed value of ϕ. But opposite trends is observed for Ψ. Differentiating Eq. (70) one can obtained the temperature gradient $T_\xi = -\lambda\left(\frac{R}{2}\Theta_\xi + \Psi_\xi\right)$. Fig. 11 depicts the effects of ϕ on Θ_ξ and Ψ_ξ for methanol and ethylene-glycol based SWCNTs and MWCNTs nano-liquid with $\gamma = -1$. It is observed from the figure that Θ_ξ is negative whereas Ψ_ξ is positive for all ξ except $\xi \neq H$. But the magnitudes of Θ_ξ and Ψ_ξ diminishes across the film thickness. A close scrutiny of the above expression of T_ξ shows that it may vanish at some height of film depending on the values of R. It can be inferred that $T_\xi = 0$ at $R = R_c$ in other word T_ξ changes its sign at $R = R_c$. Therefore, heat is transferred from the disk to nanoliquid film or nanoliquid film to rotating disk according as $T_\xi > 0$ or $T_\xi < 0$. Fig. 12 explores the change of T_ξ with R for different values of ϕ, λ and δ in methanol based SWCNTs nanoliquid for the case of heating (i.e., $\gamma = -1$). It is observed from the figure that T_ξ is positive for $0 \leq R < R_c$ and negative for $R > R_c$. Also, the values of $R = R_c$ increases for higher values of ϕ but decreases as λ increases. That is the region T_ξ for δ first increases then decreases. In Fig. 13 we have sketched the variation of R_c with ξ for different values of ϕ, λ and δ at time $\tau = 2$ in methanol based SWCNTs nanoliquid. The figure demonstrates that R_c enhances with increasing values of ϕ but it diminishes for λ and δ respectively.

6. Conclusions

CNTs nanoliquid film development over a horizontal rough rotating disk is examined. The surface of the disk is heated or cooled axisymmetrically from below. Analytical solutions for the governing set of Eqs. are obtained for small values of the Reynolds number. But these Eqs. are solved numerically for moderate values of the Reynolds number. Following conclusions may be drawn from this study.

• The nanoliquid film thickness increases with higher values of CNTs volume fraction ϕ for both SWCNTs and MWCNTs but the thickness is more for SWCNTs compare to MWCNTs.

• CNTs-nanoliquid film thinning rate enhances for higher values of radial roughness parameter λ whereas thinning rate decline for the azimuthal roughness parameter δ.

• CNTs-nanoliquid film thickness diminishes with the rising values of thermocapillary parameter α when the disk is cooling from below for the base liquids methanol, ethanol and ethylene-glycol.

• There exists a curve $R = R_c$ within the nanoliquid film which divides the region of heat transfer into two parts. In one part of the region heat flows from disk to the nanoliquid film while in other part heat flows from nanoliquid to disk.

Acknowledgment

Authors express their sincere gratitude to the Council of Scientific and Industrial Research (CSIR), New Delhi, India for the financial support with file number 25(0267)/17/ EMR-II.

References

Akbar, N.S., Nadeem, S. and Khan, Z.H. (2014), "The combined effects of slip and convective boundary conditions on stagnation-point flow of CNT suspended nanofluid over a stretching sheet", *J. Mol. Liq.* **196**, 21-25. https://doi.org/10.1016/j.molliq.2014.03.006

Akbar, N.S. and Butt, A.W. (2015), "Carbon nanotubes analysis for the peristaltic flow in curved channel with heat transfer", *Appl. Math. Comput.*, **259**, 231-241. https://doi.org/10.1016/j.amc.2015.02.052

Akbar, N.S., Raza, M. and Ellahi, R. (2015), "CNT suspended CuO + H2O nano fluid and energy analysis for the peristaltic flow in a permeable Channel", *Alex. Eng. J.*, **54**(3), 623-633. https://doi.org/10.1016/j.aej.2015.05.009

Avramenko A.A. and Shevchuk Igor, V. (2022), *Physical Foundations and Mathematical Models of Transport Processes in Nanofluids*, in *Modelling of Convective Heat and Mass Transfer in Nanofluids with and without Boiling and Condensation*, Springer, Switzerland, 1-12.

Buongiorno, J. (2006), "Convective transport in nanofluids", *J. Heat Transfer*, **128**(3), 240-250. https://doi.org/10.1115/1.2150834

Choi, S.U.S. (1995), "Enhancing thermal conductivity of fluids with nanoparticles", *Proceedings of the 1995 ASME International Mechanical Engineering Congress and Exposition*, San Francisco, USA, ASME, FED231/MD66, 99-105.

Cregan, V. and O'Brien, S.B.G. (2013), "Extended asymptotic solutions to the spin-coating model with small evaporation", *Appl. Math. Comput.*, **223**, 76-87. https://doi.org/10.1016/j.amc.2013.07.071

Dandapat, B.S. (2001), "Unsteady flow of thin liquid film on a disk under nonuniform rotation", *Phys. Fluids*, **13**, 1860-1868. https://doi.org/10.1063/1.1377615

Dandapat, B.S. and Maity, S. (2009), "Effects of air-flow and evaporation on the development of thin liquid film over a rotating annular disk", *Int. J. Non-Linear Mech.*, **44**(8), 877-882. https://doi.org/10.1016/j.ijnonlinmec.2009.06.002

Dandapat, B.S., Maity, S. and Singh, S.K. (2017), "Two-layer film flow on a rough rotating disk in the presence of air shear", *Acta Mechanica*, **228**, 4055-4065. https://doi.org/10.1007/s00707-017-1933-1

Dandapat, B.S. and Roy, P.C. (1990), "Film cooling on a rotating disk", *Int. J. Non-Linear Mech.*, **25**(5), 569-582. https://doi.org/10.1016/0020-7462(90)90019-6

Dandapat, B.S. and Roy, P.C. (1994), "The effect of themo-capillarity on the flow of a thin liquid film on a rotating disc", *J. Phys. D: Appl. Phys.*, **27**, 2041-2045.

https://doi.org/10.1088/0022-3727/27/10/009
Dandapat, B.S., Santra, B. and Kitamura, A. (2005), "Thermal effects on film development during spin coating", *Phys. Fluids*, **17**, 062102(1-6). https://doi.org/10.1063/1.1927525
Dandapat, B.S. and Singh, S.K. (2015), "Unsteady two-layer film flow on a non-uniform rotating disk in presence of uniform transverse magnetic field", *Appl. Math. Comput.*, **258**, 545-555. https://doi.org/10.1016/j.amc.2015.02.050
Ellahi, R., Zeeshan, A., Hussain, F. and Abbas, T. (2018), "Study of shiny film coating on multi-fluid flows of a rotating disk suspended with nano-sized silver and gold particles: A comparative analysis", *Coatings*, **8**(12), 422. https://doi.org/10.3390/coatings8120422
Emslie, A.C., Bonner, F.D. and Peck, L.G. (1958), "Flow of a viscous liquid on a rotating disk", *J. Appl. Phys.*, **29**, 858-862. https://doi.org/10.1063/1.1723300
Fletcher, C.A.J. (1988), *Computational Technique for Fluid Dynamics*, Springer, New York, U.S.A.
Haq, R.U., Rashid, I. and Khan, Z.H. (2017), "Effects of aligned magnetic field and CNTs in two different base fluids over a moving slip surface", *J. Mol. Liq.*, **243**, 682-688. https://doi.org/10.1016/j.molliq.2017.08.084
Higgins, B.G. (1986), "Film flow on a rotating disk", *Phys. Fluids*, **29**, 3522-3529. https://doi.org/10.1063/1.865829
Iijima, S. (1991), "Helical microtubules of graphitic carbon", *Nature*, **354**, 56-58. https://doi.org/10.1038/354056a0
Iijima, S. and Ichihashi, T. (1993), "Single-shell carbon nanotubes of 1-nm diameter", *Nature*, **363**, 603-605. https://doi.org/10.1038/363603a0
Jenekhe, S.A. and Schuldt, S.B. (1984), "Coating flow of non-Newtonian fluids on a flat rotating disk", *Ind. Eng. Chem. Fund.*, **23**(4), 432-436. https://doi.org/10.1021/i100016a009
Karpitschka, S., Weber, C.M. and Riegler, H. (2015), "Spin casting of dilute solutions: Vertical composition profile during hydro-dynamic-evaporative film thinning", *Chem. Eng. Sci.*, **129**, 243-248. https://doi.org/10.1016/j.ces.2015.01.028
Khan, M.R., Pana, K., Khanb, A.U. and Ullah, N. (2020), "Comparative study on heat transfer in CNTs-water nanofluid over a curved surface", *Int. Commun. Heat Mass Transf.*, **116**, 104707. https://doi.org/10.1016/j.icheatmasstransfer.2020.104707
Kitamura, A. (2001), "Thermal effects on liquid film flow during spin coating", *Phys. Fluids*, **13**, 2788-2794. https://doi.org/10.1063/1.1398280
Krishanan, R., Maity, S., Singh, S.K. and Dandapat, B.S. (2020), "Modelling of Thin CNTs Nano-liquid Film Flow Over a Bi-directional Stretching Surface", *Int. J. Appl. Comput. Math.*, **6**, 147. https://doi.org/10.1007/s40819-020-00900-8
Kumar, M.S., Sandeep, N. and Kumar, R.B. (2017), "Unsteady MHD nonlinear radiative squeezing slip-flow of Casson fluid between parallel disks", *J. Comput. Appl. Res. Mech. Eng.*, **7**(1), 35-45. https://doi.org/10.22061/jcarme.2017.644
Ma, F. and Hwang, J.H. (1990), "The effect of air shear on the flow of a thin liquid film over a rough rotating disk", *J. Appl. Phys.*, **68**, 1265-1271. https://doi.org/10.1063/1.346727
Maity, S. (2017), "Thermocapillary flow of thin Cu-water nanoliquid film during spin coating process", *Int. Nano Lett.*, **7**, 9-23. https://doi.org/10.1007/s40089-016-0196-5
Masuda, H., Ebata, A., Teramae, K. and Hishinuma, N. (1993), "Alterlation of thermal conductivity and viscosity of liquid by dispersing ultra-fine particles (Dispersion of g-Al2O3, SiO2, and TiO_2ultra-fine particles)", *Netsu Bussei*, **7**(4), 227-233. https://doi.org/10.2963/jjtp.7.227
Matsumoto, Y., Ohara, T., Teruya, I. and Ohashi, H. (1989), "Liquid film formation on a rotating disk", *JSME Int. J. Ser. II*, **32**(1), 52-56. https://doi.org/10.1299/jsmeb1988.32.1_52
McIntyre, A. and Brush, L.N. (2010), "Spin-coating of vertically stratified thin liquid films", *J. Fluid Mech.*, **647**, 265-285. https://doi.org/10.1017/S002211200999259X
Mouhamad, Y., Mokarian-Tabari, P., Clarke, N., Jones, R.A.L. and Geoghegan, M. (2014), "Dynamics of polymer film formation during spin coating", *J. Appl. Phys.*, **116**(12), 123513. https://doi.org/10.1063/1.4896674
Miklavčič, M. and Wang, C.Y. (2004), "The flow due to a rough rotating disk", *ZAMP*, **55**, 235. https://doi.org/10.1007/s00033-003-2096-6
Myerhofer, D.J. (1978), "Characteristics of resist films produced by spinning", *J. Appl. Phys.*, **49**(7), 3993-3997. https://doi.org/10.1063/1.325357
Niled, D.A. and Kuznetsov, A.V. (2009), "Thermal instability in a porous medium layer saturated by a nanofluid", *Int. J. Heat Mass Transf.*, **52**(25-26), 5796-5801. https://doi.org/10.1016/j.ijheatmasstransfer.2009.07.023
Peurrung, L.M. and Graves, D.B. (1991), "Film thickness profiles over topography in spin coating", *J. Electrochem. Soc.*, **138**, 2115-2124. https://doi.org/10.1149/1.2085935
Radushkevich, L. and Lukyanovich, V. (1952), "O strukture ugleroda obrazujucegosja pritermiceskomrazlozenii okisi ugleroda na zeleznom kontakte", *Zurn Fisic Chim*, **26**, 88-95.
Robert, G.O. (1971), *Lecture Notes in Physics*, Springer, New York, U.S.A.
Sahoo, S., Arora, A. and Doshi, P. (2016), "Two-layer spin coating flow of Newtonian liquids: A computational study", *Comput. Fluids*, **131**, 180-189. https://doi.org/10.1016/j.compfluid.2016.03.016
Shevchuk, I.V. (2022), "An asymptotic expansion method vs a self-similar solution for convective heat transfer in rotating cone-disk systems", *Phys. Fluids*, **34**, 103610. https://doi.org/10.1063/5.0120922
Shevchuk, I.V. (2023), "Concerning the effect of radial thermal conductivity in a self-similar solution for rotating cone-disk systems", *Int. J. Num. Methods Heat Fluid Flow*, **33**(1), 204-225. https://doi.org/10.1108/HFF-03-2022-0168
Sidik, N.A.C., Muhammad Yazid, M.N.A.W. and Samion, S. (2017), "A review on the use of carbon nanotubes nanofluid for energy harvesting system", *Int. J. Heat Mass Trans.*, **111**, 782-794. https://doi.org/10.1016/j.ijheatmasstransfer.2017.04.047
Tlili, I., Mustafa, M.T., Kumar, K.A. and Sandeep N. (2020), "Effect of asymmetrical heat rise/fall on the film flow of magnetohydrodynamic hybrid ferrofluid", *Sci. Rep.*, **10**, 6677. https://doi.org/10.1038/s41598-020-63708-y
Tlili, I., Samrat, S.P., Sandeep, N. and Nabwey, H.A. (2021), "Effect of nanoparticle shape on unsteady liquid film flow of MHD Oldroyd-B ferrofluid", *Ain Shams Eng. J.*, **12(1)**, 935-941. https://doi.org/10.1016/j.asej.2020.06.007
Turkyilmazoglu, M. (2010), "The MHD boundary layer flow due to a rough rotating disk", *Z. Angew. Math. Mech. (ZAMM)*, **90**(1), 72-82. https://doi.org/10.1002/zamm.200900259
Turkyilmazoglu, M. (2014), "Nanofluid flow and heat transfer due to a rotating disk", *Comput. Fluids*, **94**, 139-146. https://doi.org/10.1016/j.compfluid.2014.02.009
Usha, R. and Gotz, T. (2001), "Spinning of a liquid film from a rotating disc in the presence of amagnetic field: A numerical solution", *Acta Mech.* **147**, 137-151. https://doi.org/10.1007/BF01182358
Usha, R., Ravindran, R. and Uma, B. (2005), "Dynamics and stability of a thin liquid film on a heated rotating disk film with variable viscosity", *Phys. Fluids*, **17**, 102103(1-10). https://doi.org/10.1063/1.2099007
Von Kármán, T. (1921), "Uber laminare und turbulente Reibung", *Z. Angew. Math. Mech. (ZAMM)*,**1**(4), 233-252. https://doi.org/10.1002/zamm.19210010401
Wang, J., Zhu, J., Zhang, X. and Chen, Y. (2014), "Heat transfer and pressure drop of nanofluids containing carbon nanotubes in laminar flows", *Exp. Therm. Fluid Sci.* **44**, 716-721.

https://doi.org/10.1016/j.expthermflusci.2012.09.013
Washo, B.D. (1977), "Rheology and modeling of the spin coating process", *IBM J. Res. Develop.*, **21(2)**, 190-198. https://doi.org/10.1147/rd.212.0190
Wu, L. (2006), "Spin coating of thin liquid films on an axisymmetrically heated disk", *Phys. Fluids*, **18**, 063602. https://doi.org/10.1063/1.2207007

CC